Title:

FEMA: Fast and efficient mixed-effects algorithm for population-scale whole-brain imaging data

Chun Chieh Fan[*+1,2,3], Clare E Palmer[*4], John R. Iversen[4,5,6], Diliana Pecheva[2,3], Dominic Holland[3], Oleksandr Frei[7,8], Wesley K. Thompson[1,3], Donald J. Hagler, Jr.[2,3], Ole A. Andreassen[7], Terry L. Jernigan[3, 4,9, 10], Thomas E. Nichols[11, 12], Anders M. Dale[+2,3,9,13]

* Equal contribution

+ Corresponding authors

1. Population Neuroscience and Genetics Lab, University of California San Diego, USA.

2. Center for Multimodal Imaging and Genetics, University of California San Diego, USA

3. Department of Radiology, School of Medicine, University of California San Diego, USA

4. Center for Human Development, University of California San Diego, USA

5. Institute for Neural Computation, University of California San Diego, USA

6. The Swartz Center for Computational Neuroscience, University of California San Diego, USA

7. NORMENT Centre, Division of Mental Health and Addiction, Oslo University Hospital & Institute of Clinical Medicine, University of Oslo, Oslo, Norway

8. Centre for Bioinformatics, Department of Informatics, University of Oslo, Oslo, Norway

9. Department of Cognitive Science, University of California San Diego, USA

10. Department of Psychiatry, University of California San Diego, USA

11. Big Data Institute, Li Ka Shing Centre for Health Information and Discovery, Nuffield Department of Population Health, University of Oxford, Oxford, UK

12. Wellcome Centre for Integrative Neuroimaging, FMRIB, Nuffield Department of Clinical Neurosciences, University of Oxford, Oxford, UK

13. Department of Neuroscience, University of California San Diego, USA

Abstract:

The linear mixed effects model (LME) is a versatile modeling approach to deal with correlations among observations. Despite the rising importance of LME due to the complex designs of large-scale longitudinal population neuroimaging studies, LME has seldom been used in whole-brain imaging analyses due to its heavy computational requirements. Here, we introduce a fast and efficient mixed-effects algorithm (FEMA) that makes whole-brain vertexwise, voxelwise and connectome-wise LME analyses possible. In a series of realistic simulations, we demonstrate the equivalency of statistical power and control of type I errors between FEMA and classical LME, while showing orders of magnitude improvement in the computational speed. By applying FEMA on diffusion images and resting state functional connectivity matrices from the Adolescent Brain Cognitive Development Study^{SM} (ABCD) release 4.0 data, we show annualized changes in voxelwise fractional anisotropy (FA) and functional connectomes in early adolescence, highlighting a critical time of maturing connections among cortical and subcortical regions. FEMA enables researchers to quickly examine the relationships between large numbers of neuroimaging metrics and variables of interest while considering complex study designs including repeated measures and family structures.

Introduction:

As magnetic resonance imaging (MRI) studies have moved to the population scale, the size of datasets and complexity of relationships among observations have posed greater challenges to neuroimaging analyses. In the Adolescent Brain Cognitive Development (ABCD) Study^{SM}, for example, a longitudinal design and inclusion of twins and siblings make it necessary to consider correlations among observations. The flexibility of modeling random effects in the linear mixed effects model (LME) has allowed researchers to account for such repeated measures, family relatedness, and longitudinal observations (Beck et al., 2021; Bernal-Rusiel et al., 2013; Chen et al., 2013; Dick et al., 2021). Complex study designs and the heterogeneity in the study population can be parameterized by the random covariance in the LME leading to an increase in statistical power and reduction of inferential biases (Bernal-Rusiel et al., 2013). These statistical characteristics make the LME an increasingly important tool in analyzing big population data. However, there has been limited use of the LME in brain imaging studies requiring image-wise inferences (e.g. vertexwise, voxelwise, and connectome-wise), due to computational demands. Hence, the full potential of the massive population imaging samples currently collected, e.g., to reveal more of the complexity of human neurodevelopment, remains to be realized.

The classical LME requires extensive computational resources. The numeric solution for LME is typically obtained through Maximum Likelihood or Restricted Maximum Likelihood (REML) which the parametrized study covariance is iteratively inverted in order to identify the random effects that maximize the likelihood of the model (Bernal-Rusiel et al., 2013; Chen et al., 2013). Because of this procedure, the computational complexity scales polynomially with the number of data entries, making the classical solutions difficult to execute on large scale population data. It is even more challenging for whole-brain analyses, as the dependent variable can be tens of thousands of voxels, surface vertices, or

connectivities between regions of interest (ROI). Even a procedure that takes a minute to fit a single LME analysis at a single voxel would require almost a year to complete for a whole-brain voxelwise analysis. There is a need for a fast and efficient LME algorithm that is capable of handling large-scale imaging data. The release of data from the ABCD Study (Casey et al., 2018) makes this unmet need more salient, as best practices for statistical analysis are to control for cohort heterogeneity and relatedness due to the inclusion of multiple siblings and twins in the sample, in order to correctly model longitudinal measures (Dick et al., 2021; Smith and Nichols, 2018).

Previous attempts to extend LME for use in large-scale neuroimaging data analysis have relied on a divide-and-conquer approach (Bernal-Rusiel et al., 2013; Chen et al., 2013). For example, the LME toolbox for longitudinal analyses released with Freesurfer starts cortical surface vertexwise LME by segmenting vertices into a smaller set of regions of interest that share similar random effects and are geodesically close, thus reducing the number of outcome variables and the size of the covariance matrix whose inverse must be calculated (Bernal-Rusiel et al., 2013). However, it currently lacks support for complex study design, such as inclusion of family members, and imaging measures beyond cortical surfaces. The LME tool implemented in AFNI utilizes the parallelization by performing multiple threads of the LME solver in R (from the lme4 package) to derive the results (Chen et al., 2013). It quickly becomes infeasible for large-scale population imaging data with thousands of dependent variables. The core of both Freesurfer LME and AFNI LME is REML which still needs polynomial time to estimate the parameterized covariances. Finally, one approach to make mixed effects modelling practical for neuroimaging is to fit only a marginal model and rely on a sandwich estimator of standard errors to incorporate repeated measures covariance. The SwE toolbox takes this approach, using a working covariance of independence it fits an ordinary least squares regression but then estimates intra-block covariance when conducting inference (Guillaume et al., 2014). Although SwE is computationally

efficient and produces valid inferences, a LME model would be more efficient in whitening data and model, leading to improvement in the statistical power.

Here, we present a fast and resource efficient LME algorithm, called the Fast and Efficient Mixed-effects Algorithm (FEMA), that can perform whole-brain image-wise analyses on complex large-scale imaging data in a computationally efficient manner. By utilizing the method-of-moments estimator, effect binning, and sparsity of the random effects design matrices, FEMA finishes whole-brain image-wise LME analyses within minutes, compared to days or even months required using REML solvers, thus allowing the analyses to be run using ordinary computer without the need for large memories or extensive parallelization. Using both realistically simulated data and empirical data from the ABCD Study, we have demonstrated that the results from FEMA are consistent with classical REML results while the required resources and computational times are dramatically reduced, allowing researchers to quickly examine the relationships between neuroimaging metrics and variables of interest while considering repeated measures, family structures, and other complex study designs. Applying FEMA to longitudinal multimodal brain imaging data of the ABCD Study revealed the neurodevelopmental patterns of human brain change during early adolescence regarding tissue microstructure and resting-state functional connectivity networks.

Material and Methods

Figure 1 illustrates the algorithmic design of FEMA in three steps. First, FEMA sets up the model as a classical LME with random intercept that characterizes the variation within and between groups. As an example, we use an intercept with three independent components that characterizes the variance attributable to the family relatedness (F), the variance attributable to individual subjects (S), and the

measurement errors (E) (Figure 1, panel I). Second, the random effects are estimated through moment-estimators instead of classical maximum likelihood approach, utilizing the benefit of large sample size and sparse indicator matrices (Figure 1, panel II). Third, the fixed effects are estimated by generalized least squares given the estimated random effects, leveraging binning of the random effects into finite discrete configurations to reduce the number of parameterized covariance matrix inversions (Figure 1, panel III). In the following section, we elaborate each of these three steps.

Model Set Up

As in most of the classical analytic approaches in brain mapping, we assume an additive linear relationship between imaging measures (y) and covariates of interest (x) plus random variations (μ), as

$$y_{ij} = x_i\beta_j + \mu_{ij} \#(1)$$

for $i \in 1..N$ observations and $j \in 1..J$ imaging measures (voxels/vertices/connectivities), and $x_i\beta_j$ is the dot product of a vector of covariates with a vector of fixed effects. We follow a mass-univariate approach where we will not attempt to model the dependence between the J imaging measures, but we will combine information across the measures to obtain reliable variance parameter estimates.

In the fixed effects only setting (e.g. simple linear regression model, LM) or marginal models (e.g. generalized estimating equation), μ accounts for the marginal errors. The LME, on the other hand, assumes the random term, μ, captures not only the uncorrelated measurement error but in addition correlations among observations attributable to the known structure of the data entries. We assume it is normally distributed, for each imaging measure, j

$$\mu_j \sim N(0, V_j) \#(2)$$

For example, given the longitudinal design and inclusion of family members, random intercepts for subject and family induce a marginal variance structure V_j that can be parameterized as the variance attributable to living in the same family (F), repeated measures from the same subject (S), and random errors (E), assumed to be independent and have compound symmetry:

$$V_j = \sigma_{j,F}^2 Z_F Z_F' + \sigma_{j,S}^2 Z_S Z_S' + \sigma_{j,E}^2 I \# (3)$$

where, generically, Z is an indicator matrix expressing the random intercepts, where row z_i specifies the membership of i-th observation, and each column corresponds to a different level of the random factor, Z_F for families, Z_S for subjects, each with a corresponding variance parameter, $\sigma_{j,F}^2$ and $\sigma_{j,S}^2$, respectively; $\sigma_{j,E}^2$ is the variance of the random uncorrelated measurement error. Echoing to the model set up in equation (1), the random intercepts can be rewritten in matrix form as $\mu_j = Z_F \mu_{j,F} + Z_S \mu_{j,S} + I \mu_{j,E}$ using random effects vectors $\mu_{F,j}$ and $\mu_{S,j}$ with dimension equal to the number of families and the number of individuals, respectively.

The main computational bottleneck here is the estimation of V_j for every imaging outcome measure, as the computational complexity is at least $O(n^2)$ in the number of observations, n, if REML is used for each imaging measure. When the number of imaging measures, J, is large, such as voxelwise analyses, solving REML for every single measure would be computationally infeasible. In the following section, we discuss how our algorithm overcomes this computational limitation.

<u>Estimating the variance components</u>

To overcome the computational bottleneck of estimating the parameterized covariance matrix, V_j, we implemented the method of moments estimator to obtain the values of $\sigma_{j,F}^2$ and $\sigma_{j,S}^2$ for each voxel j, which is fast and unbiased with some sacrifice on statistical efficiency, as it is generally the case for

MoM vs ML estimators (Ge et al., 2016; Haseman and Elston, 1972). For a given voxel j and for each pair of observations (i, i') the expected value of the product of corresponding residuals $\hat{y}_{j,i}^{res}$ and $\hat{y}_{j,i'}^{res}$ is:

$$E\left[\hat{y}_{j,i}^{res}\hat{y}_{j,i'}^{res}\right] = \sigma_{j,F}^2(Z_F Z_F')_{i,i'} + \sigma_{j,S}^2(Z_S Z_S')_{i,i'} + \sigma_{j,E}^2, \#(4)$$

where the residual vector is computed as $\hat{Y}_j^{res} = Y_j - X\hat{B}_j$, $\hat{B}_j = (X'X)^{-1}X'Y_j$, the E operator represents the expectation with respect to random effects, and $(ZZ')_{i,i'}$ denotes the (i, i') element of the ZZ' matrix. Eqn. (2) specifies $n(n-1)/2$ equations with 3 unknowns, allowing us to estimate the variance parameters using ordinary least squares (OLS). Crucially, the OLS estimates can be expressed as a simple matrix expression allowing us to simultaneously obtain the variance parameters for all voxels/vertices. Given the marginal variance is highly structured, as the indicator matrices are sparse and have only a small number of possible configurations, the OLS procedure can be further simplified (Chen et al., 2019). However, in our current implementation of FEMA, we kept the general form of solving $n(n-1)/2$ equations as the matrix multiplications enable the simultaneous mass-univariate estimations across J measures.

<u>Estimating fixed effects for the variables of interest</u>

Once the three variance parameters are estimated for each j, the covariance matrix V_j can be composed per Eq. (3), and fixed effects estimated with generalized least squares:

$$\hat{\beta}_j = \left(X'V_j^{-1}X\right)^{-1}X'V_j^{-1}y_j \#(5)$$

with variance

$$Var\left(\hat{\beta}_j\right) = \left(X'V_j^{-1}X\right)^{-1} \#(6)$$

The test statistic for individual fixed effects is then computed as Wald's ratio, $\frac{\hat{\beta}_j}{se(\hat{\beta}_j)}$. For an arbitrary contrast estimate $C = c'\hat{\beta}_j$Wald's ratio is computed using $Var(C) = c'Var(\hat{\beta})c$.

To further speed up the calculations, instead of separately inverting parameterized covariance, V_j, for each of J imaging measures, we grouped them on a regular multidimensional grid according to the values of estimated random effects, binning $\hat{\sigma}^2_{j,F}$, $\hat{\sigma}^2_{j,S}$ and $\hat{\sigma}^2_{j,E}$ into only K sets of values, where K << J. In a series of simulations, we will show how a finite number of gridded bins is sufficient to capture the variance components for all input imaging measures while dramatically reducing the required computational time.

<u>Simulations</u>

To evaluate the validity of our algorithm, we performed simulations with realistic data generated from random effects models and covariance structure from the imaging data of ABCD Study. The ABCD Study is a longitudinal study across 21 sites following 11,880 individuals starting at 9-11 years old, with epidemiologically informed ascertainment and incorporation of a family component, including monozygotic twins, dizygotic twins, and siblings in the study samples (Casey et al., 2018). Given the complexity of the ABCD data, we utilized its data structure to simulate realistic scenarios of large-scale population imaging studies. Here, we randomly sampled covariates, repeated observations, and family indices from the real ABCD data. The forward simulations assume

$$y_{ij} = x_i\beta_j + \mu_{ij}$$

$$x \sim N(0, 1)$$

$$\mu_j \sim N(0, V_j)$$

$$V_j = \sigma^2_{j,F} Z_F Z_F' + \sigma^2_{j,S} Z_S Z_S' + \sigma^2_{j,E} I \#(7)$$

where the fixed and random effects parameters were sampled as:

$$\beta_j \sim unif(-0.02,0.02)$$

$$\sigma_j^2 \sim unif(0.2,0.8)$$

$$\sigma_{j,F}^2 + \sigma_{j,S}^2 + \sigma_{j,E}^2 = 1\#(8)$$

The range of the parameters were chosen based on the observations reported in large-scale imaging analyses, i.e. small effect sizes and evident effects of family and repeated measures (Dick et al., 2021). We then forward simulated the imaging measures y, based on the sampled covariates and variance components defined by subject indices (S) and family indices (F). We randomly generated the true values of variance parameters and the fixed effects coefficients to see how different variance component values would impact the validity and accuracy of the estimation of the parameters of interest. In each simulation scenario, we simultaneously generated 5000 imaging measures, with randomly assigned parameters for each imaging measure. The β_j were set to 0 when we specifically examined the Type I error rates. We repeated the simulations in two runs per scenario, resulting in simulating 10,000 random imaging measures in each scenario. We then compared our FEMA with REML based LME (REML-LME) in terms of: 1) validity and reliability of the fixed effects estimation; 2) the computational cost of the algorithms; and, 3) the impact of model misspecification, i.e. providing fewer numbers of random effects configurations.

Empirical Application

To demonstrate the utility of FEMA, we applied our method to ABCD data release 4.0 to examine longitudinal changes in imaging measures during adolescence. The longitudinal images were collected 2 years after the baseline imaging scans. The ABCD Study utilized multi-modal imaging protocols, including structural T1 images, multi-shell diffusion images, functional task MRI, and resting state

functional MRI (Casey et al., 2018; Hagler et al., 2019). In our empirical application to showcase FEMA, we focused on two imaging measurements: fractional anisotropy (FA) from diffusion MRI and connectivities from resting-state functional MRI. Details of image processing and quality controls can be found elsewhere (Hagler et al., 2019). FA derived from diffusion MRI reflects the underlying micro-structural properties of the tissues (Tournier et al., 2011). The connectivities are the BOLD signal correlations between brain regions, including functionally defined cortical parcels (Gordon et al., 2016) and anatomically defined subcortical regions (Fischl et al., 2002), during resting-state functional MRI scans. We investigated how voxelwise diffusion imaging measures and resting-state connectivity measures changed over time as ABCD participants matured. In our analyses, the family IDs and subject IDs were treated as indicators for random intercepts (Figure 1, panel I for example), capturing the variance attributable to shared family relatedness and the within-person longitudinal stabilities (Dick et al., 2021). The confounding variables include age-at-enrollment, sex, population structure (first 10 genetic principal components), MRI scanner, MRI software versions, parental incomes, and parental education levels. The variable of interest was the difference in age between the first imaging scan and the second imaging scan, allowing us to examine how the imaging measures changed over development. Given that for both imaging modalities there are more than 100K voxels or between ROI connectivities, it is infeasible to apply classical LME for these datasets. Therefore, we only compared FEMA with naive applications of simple linear models (LM), highlighting the benefit of having a fast and efficient LME solver. To showcase the improvement of power of FEMA compared to LM, we calculated the relative efficiency as the ratio of effective sample sizes:

$$Efficiency = \frac{N_{FEMA}}{N_{LM}} = \frac{Var(\beta_{LM})}{Var(\beta_{FEMA})}$$

Because the estimation of the effective sample size is taking the $Var(\beta_{LM})$ as the nominator, which is negatively biased by failing to taking into consideration of family and subject dependence, this is a conservative comparison in terms of improvement in relative efficiency by using FEMA. For example, a relative efficiency of 2 means that a naive LM analysis would require twice or more the sample size to obtain the same accuracy as we obtain with FEMA.

Results:

Simulations

Compared to REML-LME, FEMA dramatically reduced the computational time without using parallel processing (Figure 2a). With data entries equivalent to ABCD release 4.0 (n = 18K), FEMA obtained results from 5000 voxels within seconds, whereas the REML solver required more than 33 hours to finish (Figure 2b). Meanwhile, the statistical power was equivalent between FEMA and REML-LME across different sizes of input observations (Figure 2b). The type I errors were well controlled for both FEMA and REML-LME regardless of the underlying true number of random effects configurations, despite that effect binning being held constant at 20 (Figure 2c). When we simulated the scenario of mis-specifying the number of random effects in FEMA, such as using K = 20 for 5000 voxels with 100 different random effects, the estimated fixed effects were still robust (Figure 2d). Even with K much smaller than the number of true random effect configurations (100), the mean squared errors are almost the same as for the LME. The differences were negligible compared to the range of true values (differences in MSE: < 1e-7, true coefficient value range: -0.02 ~ 0.02). On the other hand, since the computational time of FEMA only scales linearly with the number of bins (Supplementary Figure 1), users can increase the resolutions of random effects without worrying about the feasibility of analyzing whole-brain data.

Empirical results - developmental changes on fractional anisotropy across voxels

To showcase the utility of FEMA, we performed voxelwise analysis on a measure derived from diffusion MRI data of ABCD release 4.0. We examined the rate of change in FA while controlling for age at recruitment, sex, scanner, household income, highest parental education, and first 10 genetic principal components. The variable of interest in the regression model is the change of age between two scans. The subject-wise repeated measures (S) and family relatedness (F) were specified as random intercepts in FEMA. Despite large numbers of voxels (100x100x130), eligible observations (n=13,428 entries), clusters of families (N = 8197), and repeated imaging scans (5,022 second scans), FEMA finished the analyses in 60 seconds without the use of parallel computing. The estimated random effects indicate modest family effects across voxels and large variations in longitudinal stability (Figure 3A). The random effects have distinct anatomical distributions despite no spatial priors being used in the estimation process (Figure 3B for the variance in longitudinal stability, S, and Figure 3C for the variance in family effects, F). Removing the F and S variability from the residuals results in improvement of statistical power, and the voxels with high family effects or longitudinal stability benefit the most; relative efficiency increases two-fold in the majority (Figure 3D). For the fixed effects, the annualized rate of change in FA was most evident within the bilateral cingulum (Figure 3E), many voxels of which survived the multiple comparison corrected threshold (p = 0.01/total number of voxels = 7.7e-9; Figure 3F).

Empirical results - developmental changes on resting state functional connectivities across cortical and subcortical regions

The versatility of FEMA also allows us to examine the annualized rate of change in resting state connectivities (cortical parcels and subcortical regions, Figure 4). With the same model configuration as the voxelwise analysis on FA, we examined how the resting state connectivities across cortical and subcortical regions changed over time (582 ROIs in total, J = 169071 unique connectivities). FEMA showed that the resting state connectivities had relatively low family effects and modest longitudinal stability (Figure 4A). Nevertheless, the inference on the fixed effect of annualized rate of change still benefited from having the S and F partitioned out from the residuals (Figure 4B). As shown in Figure 4C and 4D, both S and F seem to follow the modularization of the connectivity groups, also referred to as functional networks or communities (Baria et al., 2011; Gordon et al., 2016; Gordon et al., 2020) . The rate of change was most evident in the connections within networks (Figure 4E), as increased connectivities with age within each network were statistically significant after Bonferroni correction. Several between-network connectivities were also significantly increased, such as between somatomotor regions and auditory/visual cortices, and between cingulate and dorsal attention regions, reflecting the ongoing cross modular integration during this developmental period.

Discussion

The aim of the study was to develop and validate the FEMA tool as a way to make whole brain LME analyses feasible. We have shown that, while the statistical power and type I errors are equivalent between FEMA and REML-LME, the computational times were dramatically reduced in FEMA, making it possible to perform large scale, whole brain imaging analyses quickly and efficiently, regardless of imaging modality. FEMA is robust to model misspecification and when there is strong evidence for family effects and longitudinal stabilities, FEMA can greatly improve power for statistical inference by partitioning out this variability from the residual errors.

Applying the FEMA tool to longitudinal multimodal brain imaging data with more than 13K observations showed an interesting pattern of human brain changes throughout early adolescent development in terms of tissue microstructure (Figure 3) and resting-state functional connectivity networks (Figure 4). For both imaging modalities, there were widespread changes with age across the brain, highlighting the benefit of using a voxelwise analysis.

A further benefit of using FEMA is that we can map the estimated family and subject random effects across the brain. Longitudinal stability showed larger effects compared to family for both modalities. For FA, voxels nearer the cortical surface showed greater longitudinal stability than voxels more inferior in the brain and across subcortical regions. This potentially highlights how the microstructure of the cortical sheet may act as a unique 'fingerprint' afforded to each subject that is stable over time. Subcortical voxels showed greater family effects, which may highlight that FA in these regions is either heritable or is related to experiencing a common environment. With this model design, it is difficult to tease apart these factors, as our measure of family is based only on whether individuals belong to the same family unit. Future work will aim to incorporate genetic relatedness and other environmental data to better partition these random effects. The resting-state functional connectivity networks showed a similar difference in random effect sizes as FA, i.e., higher longitudinal stability than family effects, across multiple networks. The dorsal attention, fronto-parietal and visual attention networks appeared to show the greatest longitudinal stability, highlighting that connectivity within these networks may be particularly reliable within an individual over early adolescence.

To conclude, FEMA yields statistical power and control of type I errors equivalent to classical LME, while the computational speed is improved by orders of magnitude. We found annualized changes in voxelwise FA and functional connectomes in early adolescence, highlighting a critical time of maturing connections among cortical and subcortical regions. We were further able to examine the

topographical patterns of longitudinal stability and family effects. These results demonstrate the potential of FEMA, which enables researchers to rapidly examine the relationships between voxelwise neuroimaging metrics and variables of interest while considering repeated measures, family structures, and complex study designs as those arising from repeated measures and family structures.

Code Availability

FEMA is publicly available on github (https://github.com/cmig-research-group/FEMA). The development version can be obtained by sending the request to authors.

Data Availability

Adolescent data used in the preparation of this article were obtained from the Adolescent Brain Cognitive Development Study (ABCD Study®) (https://abcdstudy.org), held in the NIMH Data Archive (NDA).

Acknowledgement

This work was supported by grant R01MH122688, RF1MH120025, and R01MH118281 funded by the National Institute for Mental Health (NIMH). Data used in the preparation of this article were obtained from the Adolescent Brain Cognitive DevelopmentSM(ABCD) Study (https://abcdstudy.org), held in the NIMH Data Archive (NDA). The ABCD Study® is supported by the National Institutes of Health and additional federal partners under award numbers U01DA041048, U01DA050989, U01DA051016, U01DA041022, U01DA051018, U01DA051037, U01DA050987, U01DA041174, U01DA041106, U01DA041117, U01DA041028, U01DA041134, U01DA050988, U01DA051039, U01DA041156,

U01DA041025, U01DA041120, U01DA051038, U01DA041148, U01DA041093, U01DA041089, U24DA041123, U24DA041147. A full list of supporters is available at https://abcdstudy.org/federal-partners.html. A listing of participating sites and a complete listing of the study investigators can be found at https://abcdstudy.org/consortium_members/. ABCD consortium investigators designed and implemented the study and/or provided data but did not necessarily participate in the analysis or writing of this report. This manuscript reflects the views of the authors and may not reflect the opinions or views of the NIH or ABCD consortium investigators. The ABCD data repository grows and changes over time. The ABCD data used in this report came from DOI: 10.15154/1524729. The fast track data release used in this report are available at https://nda.nih.gov/edit_collection.html?id=2573. Instructions on how to create an NDA study are available at https://nda.nih.gov/training/modules/study.html).

Conflict of Interest

Dr. Dale is a Founder of and holds equity in CorTechs Labs, Inc, and serves on its Scientific Advisory Board. He is a member of the Scientific Advisory Board of Human Longevity, Inc. and receives funding through research agreements with General Electric Healthcare and Medtronic, Inc. The terms of these arrangements have been reviewed and approved by UCSD in accordance with its conflict of interest policies. The other authors declare no competing interests.

Figure Legends

Figure 1. Estimation procedures of FEMA. First panel illustrates the example of model set up, with random effects from family (F), repeated measures (S), and random errors (E). The second step involves estimating the random effects through moment estimator (Panel II). After binning voxels/images into K groups, the fixed effects are derived via weighted least square (Panel III).

Figure 2. Results from simulations. Red indicates results from FEMA. Blue are results from REML-LME. **A.** CPU time as a function of sample size, estimating 5000 voxels. **B.** Statistical power of detecting effect with Cohen's d greater than 0.005. The blue and red lines/dots are overlapping with each other, showing no distinction between two approaches. **C.** Type I errors given different number of true random effect configurations, holding the binning number constant at 20. **D.** Mean square errors of the fixed effects as a function of number of random effects bins, holding the true number of random effect configurations at 100.

Figure 3. Rate of changes on fractional anisotropy (FA) among ABCD participants. A. Distribution of random effects on FA across all voxels. F is the variations attributable for living in the same family; S is the subject specific variations, capturing the longitudinal stability of a given measurement; E is the independent random errors. **B.** Spatial distribution of S. **C.** Spatial distribution of F. **D.** The improvement of the power comparing FEMA to LM, as a function of S+F. The x axis is the sum of the S and F while the y axis is the relative efficiency. Larger the ratios indicate better in the statistical power. **E.** Effect size distribution of the rate of change on FA across major fiber tracts. The distribution of Z statistics was grouped based on the location of the voxels on the major fiber tracts, showing as gray

colored violin plots in panel F. The corresponding Bonferroni threshold is shown by the red dashed lines in the plot.

Figure 4. Rate of changes on resting state connectivities among ABCD participants. **A.** Distribution of random effects on the connectivities across all cortical parcels and subcortical regions. F is the variations attributable for living in the same family; S is the subject specific variations, capturing the longitudinal stability of a given measurement; E is the independent random errors. **B.** Distribution of S across connectomes, grouped according to the functional networks. **C.** Distribution of F. **D.** The improvement of the power comparing FEMA to LM, as a function of S+F. The x axis is the sum of the S and F while the y axis is the relative efficiency. Larger ratios indicate better statistical power. **E.** Effect size distribution of the rate of change on connectivity across brain regions, grouped according to the functional networks. The associations have been threshold according to the significance level in 0.05 after Bonferroni correction.

Figure 1.

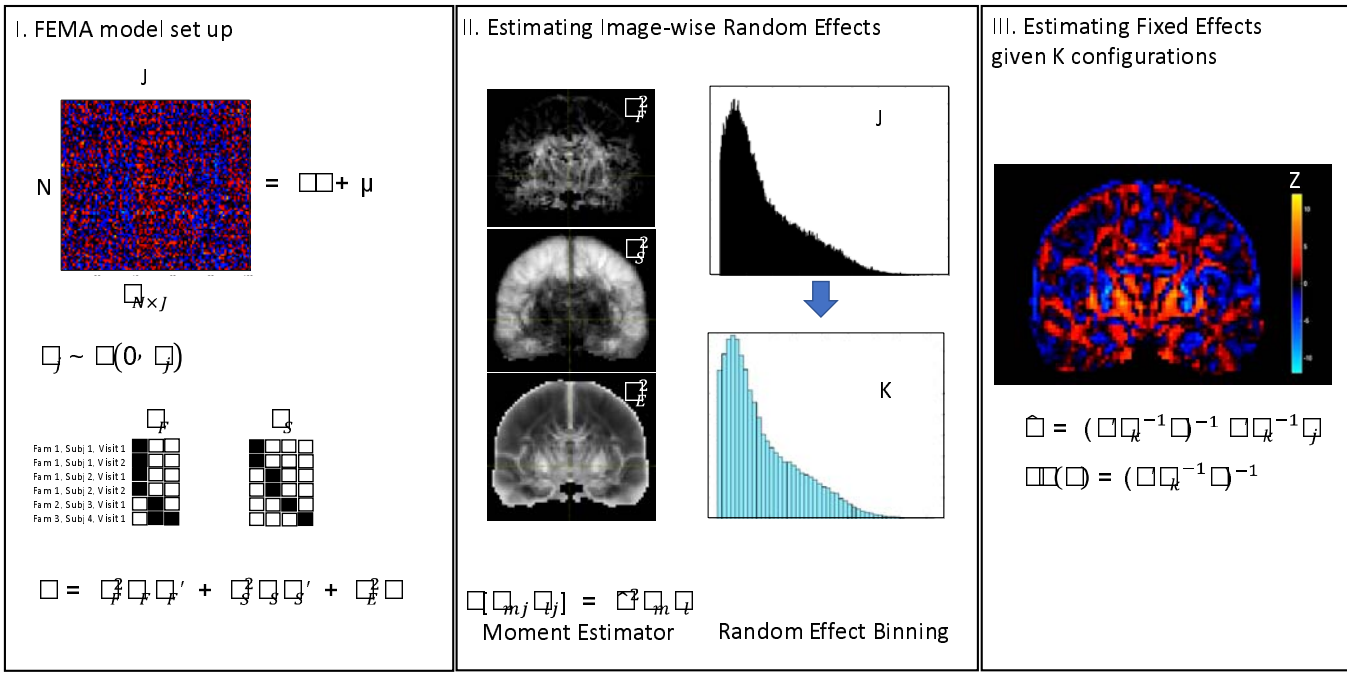
I. FEMA model set up
J
N
= + μ
Fam 1, Subj 1, Visit 1
Fam 1, Subj 1, Visit 2
Fam 1, Subj 2, Visit 1
Fam 1, Subj 2, Visit 2
Fam 2, Subj 3, Visit 1
Fam 3, Subj 4, Visit 1
II. Estimating Image-wise Random Effects
J
K
Moment Estimator
Random Effect Binning
III. Estimating Fixed Effects given K configurations
Z

Figure 2.

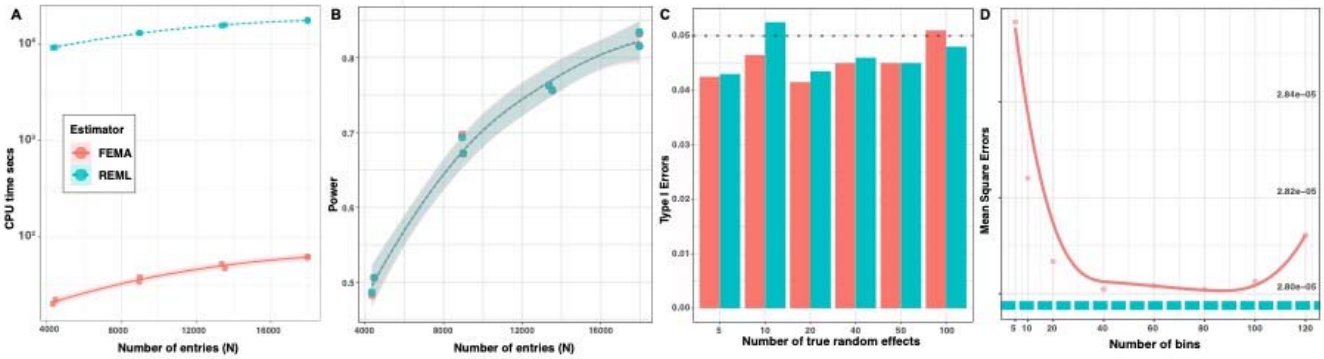
A
CPU time secs
Estimator
FEMA
REML
Number of entries (N)
B
Power
Number of entries (N)
C
Type I Errors
Number of true random effects
D
Mean Square Errors
2.84e-05
2.82e-05
2.80e-05
Number of bins

Figure 3

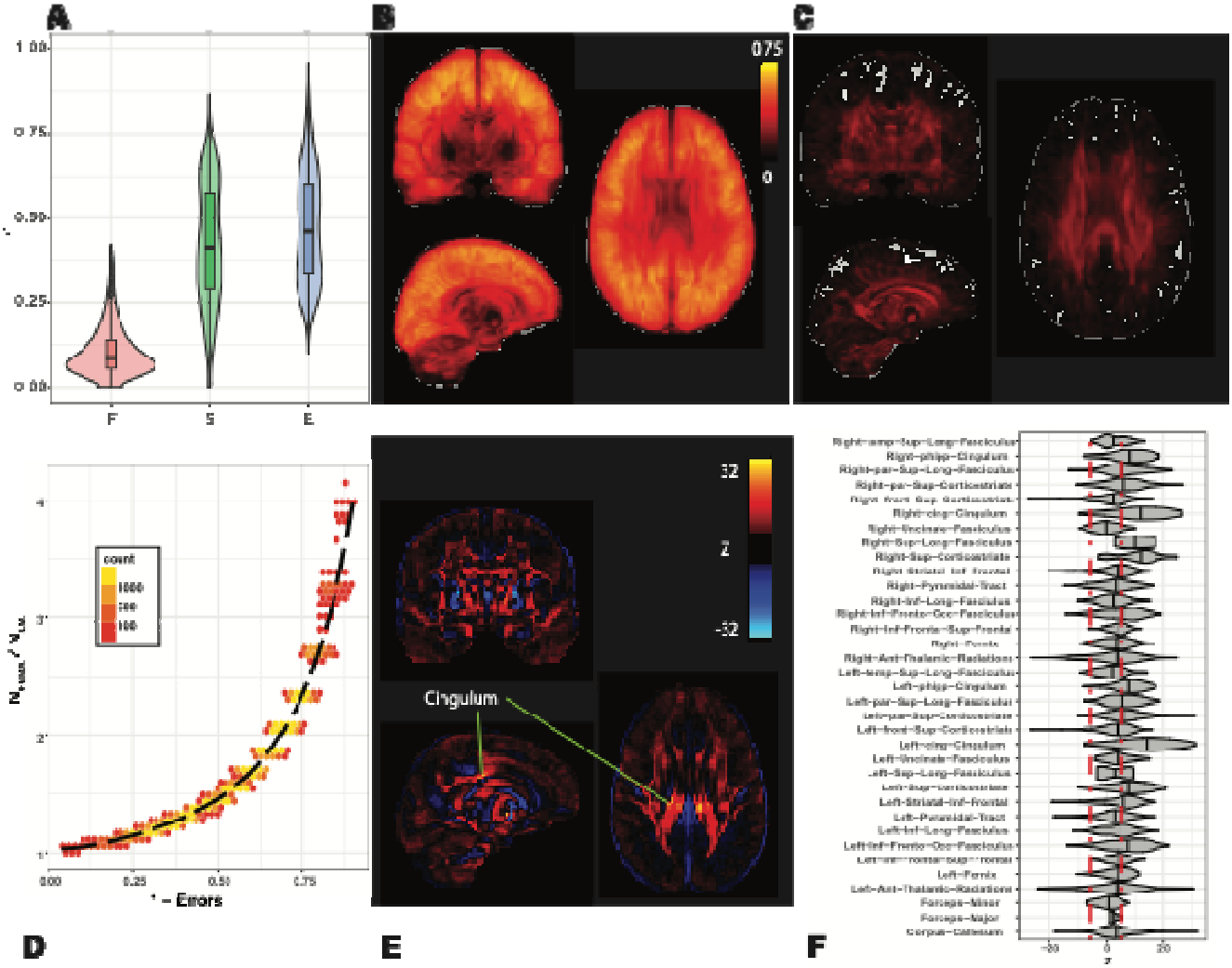

Figure 4

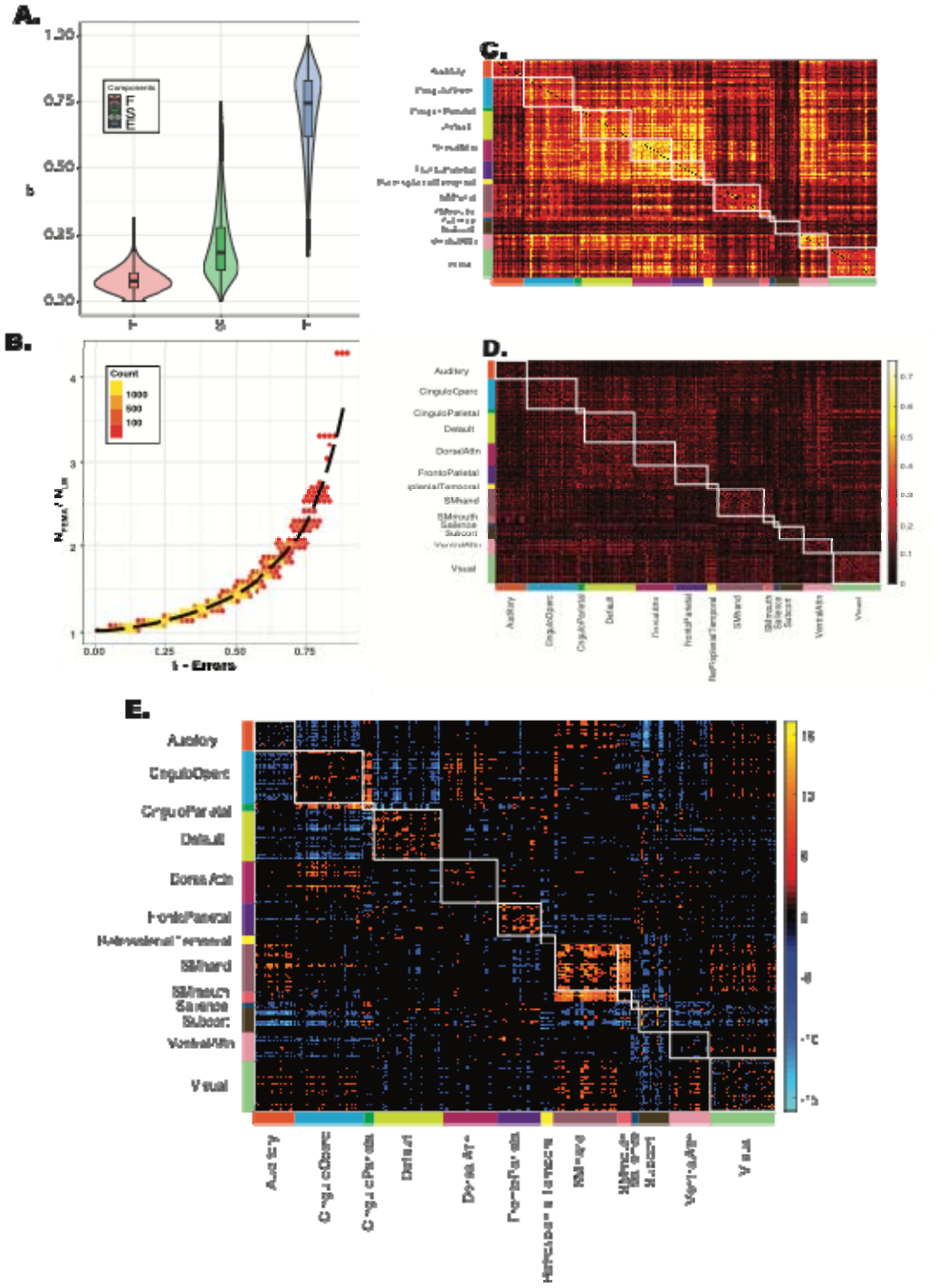
A.
B.
C.
D.
E.
Count
1000
500
100
1 - Errors
Auditory
CingulOperc
CingulParietal
Default
DorsalAttn
FrontoParietal
SMhand
Visual

References

Baria, A.T., Baliki, M.N., Parrish, T., Apkarian, A.V., 2011. Anatomical and functional assemblies of brain BOLD oscillations. J Neurosci 31, 7910-7919.

Beck, D., de Lange, A.G., Maximov, I.I., Richard, G., Andreassen, O.A., Nordvik, J.E., Westlye, L.T., 2021. White matter microstructure across the adult lifespan: A mixed longitudinal and cross-sectional study using advanced diffusion models and brain-age prediction. Neuroimage 224, 117441.

Bernal-Rusiel, J.L., Greve, D.N., Reuter, M., Fischl, B., Sabuncu, M.R., Initiative, A.s.D.N., 2013. Statistical analysis of longitudinal neuroimage data with Linear Mixed Effects models. Neuroimage 66, 249-260.

Casey, B.J., Cannonier, T., Conley, M.I., Cohen, A.O., Barch, D.M., Heitzeg, M.M., Soules, M.E., Teslovich, T., Dellarco, D.V., Garavan, H., Orr, C.A., Wager, T.D., Banich, M.T., Speer, N.K., Sutherland, M.T., Riedel, M.C., Dick, A.S., Bjork, J.M., Thomas, K.M., Chaarani, B., Mejia, M.H., Hagler, D.J., Jr., Daniela Cornejo, M., Sicat, C.S., Harms, M.P., Dosenbach, N.U.F., Rosenberg, M., Earl, E., Bartsch, H., Watts, R., Polimeni, J.R., Kuperman, J.M., Fair, D.A., Dale, A.M., Workgroup, A.I.A., 2018. The Adolescent Brain Cognitive Development (ABCD) study: Imaging acquisition across 21 sites. Dev Cogn Neurosci 32, 43-54.

Chen, G., Saad, Z.S., Britton, J.C., Pine, D.S., Cox, R.W., 2013. Linear mixed-effects modeling approach to FMRI group analysis. Neuroimage 73, 176-190.

Chen, X., Formisano, E., Blokland, G.A.M., Strike, L.T., McMahon, K.L., de Zubicaray, G.I., Thompson, P.M., Wright, M.J., Winkler, A.M., Ge, T., Nichols, T.E., 2019. Accelerated estimation and permutation inference for ACE modeling. Hum Brain Mapp 40, 3488-3507.

Dick, A.S., Lopez, D.A., Watts, A.L., Heeringa, S., Reuter, C., Bartsch, H., Fan, C.C., Kennedy, D.N., Palmer, C., Marshall, A., Haist, F., Hawes, S., Nichols, T.E., Barch, D.M., Jernigan, T.L., Garavan, H., Grant, S., Pariyadath, V., Hoffman, E., Neale, M., Stuart, E.A., Paulus, M.P., Sher, K.J., Thompson, W.K., 2021. Meaningful associations in the adolescent brain cognitive development study. Neuroimage 239, 118262.

Fischl, B., Salat, D.H., Busa, E., Albert, M., Dieterich, M., Haselgrove, C., van der Kouwe, A., Killiany, R., Kennedy, D., Klaveness, S., Montillo, A., Makris, N., Rosen, B., Dale, A.M., 2002. Whole brain segmentation: automated labeling of neuroanatomical structures in the human brain. Neuron 33, 341-355.

Ge, T., Reuter, M., Winkler, A.M., Holmes, A.J., Lee, P.H., Tirrell, L.S., Roffman, J.L., Buckner, R.L., Smoller, J.W., Sabuncu, M.R., 2016. Multidimensional heritability analysis of neuroanatomical shape. Nat Commun 7, 13291.

Gordon, E.M., Laumann, T.O., Adeyemo, B., Huckins, J.F., Kelley, W.M., Petersen, S.E., 2016. Generation and Evaluation of a Cortical Area Parcellation from Resting-State Correlations. Cereb Cortex 26, 288-303.

Gordon, E.M., Laumann, T.O., Marek, S., Raut, R.V., Gratton, C., Newbold, D.J., Greene, D.J., Coalson, R.S., Snyder, A.Z., Schlaggar, B.L., Petersen, S.E., Dosenbach, N.U.F., Nelson, S.M., 2020. Default-mode network streams for coupling to language and control systems. Proc Natl Acad Sci U S A 117, 17308-17319.

Guillaume, B., Hua, X., Thompson, P.M., Waldorp, L., Nichols, T.E., Initiative, A.s.D.N., 2014. Fast and accurate modelling of longitudinal and repeated measures neuroimaging data. Neuroimage 94, 287-302.

Hagler, D.J., Hatton, S., Cornejo, M.D., Makowski, C., Fair, D.A., Dick, A.S., Sutherland, M.T., Casey, B.J., Barch, D.M., Harms, M.P., Watts, R., Bjork, J.M., Garavan, H.P., Hilmer, L., Pung, C.J., Sicat, C.S.,

Kuperman, J., Bartsch, H., Xue, F., Heitzeg, M.M., Laird, A.R., Trinh, T.T., Gonzalez, R., Tapert, S.F., Riedel, M.C., Squeglia, L.M., Hyde, L.W., Rosenberg, M.D., Earl, E.A., Howlett, K.D., Baker, F.C., Soules, M., Diaz, J., de Leon, O.R., Thompson, W.K., Neale, M.C., Herting, M., Sowell, E.R., Alvarez, R.P., Hawes, S.W., Sanchez, M., Bodurka, J., Breslin, F.J., Morris, A.S., Paulus, M.P., Simmons, W.K., Polimeni, J.R., van der Kouwe, A., Nencka, A.S., Gray, K.M., Pierpaoli, C., Matochik, J.A., Noronha, A., Aklin, W.M., Conway, K., Glantz, M., Hoffman, E., Little, R., Lopez, M., Pariyadath, V., Weiss, S.R., Wolff-Hughes, D.L., DelCarmen-Wiggins, R., Feldstein Ewing, S.W., Miranda-Dominguez, O., Nagel, B.J., Perrone, A.J., Sturgeon, D.T., Goldstone, A., Pfefferbaum, A., Pohl, K.M., Prouty, D., Uban, K., Bookheimer, S.Y., Dapretto, M., Galvan, A., Bagot, K., Giedd, J., Infante, M.A., Jacobus, J., Patrick, K., Shilling, P.D., Desikan, R., Li, Y., Sugrue, L., Banich, M.T., Friedman, N., Hewitt, J.K., Hopfer, C., Sakai, J., Tanabe, J., Cottler, L.B., Nixon, S.J., Chang, L., Cloak, C., Ernst, T., Reeves, G., Kennedy, D.N., Heeringa, S., Peltier, S., Schulenberg, J., Sripada, C., Zucker, R.A., Iacono, W.G., Luciana, M., Calabro, F.J., Clark, D.B., Lewis, D.A., Luna, B., Schirda, C., Brima, T., Foxe, J.J., Freedman, E.G., Mruzek, D.W., Mason, M.J., Huber, R., McGlade, E., Prescot, A., Renshaw, P.F., Yurgelun-Todd, D.A., Allgaier, N.A., Dumas, J.A., Ivanova, M., Potter, A., Florsheim, P., Larson, C., Lisdahl, K., Charness, M.E., Fuemmeler, B., Hettema, J.M., Maes, H.H., Steinberg, J., Anokhin, A.P., Glaser, P., Heath, A.C., Madden, P.A., Baskin-Sommers, A., Constable, R.T., Grant, S.J., Dowling, G.J., Brown, S.A., Jernigan, T.L., Dale, A.M., 2019. Image processing and analysis methods for the Adolescent Brain Cognitive Development Study. Neuroimage 202, 116091.

Haseman, J.K., Elston, R.C., 1972. The investigation of linkage between a quantitative trait and a marker locus. Behav Genet 2, 3-19.

Smith, S.M., Nichols, T.E., 2018. Statistical Challenges in "Big Data" Human Neuroimaging. Neuron 97, 263-268.

Tournier, J.D., Mori, S., Leemans, A., 2011. Diffusion tensor imaging and beyond. Magn Reson Med 65, 1532-1556.